

Airborne and Ground Monitors for Ionospheric Front Detection for the Local Area Augmentation System Using Carrier Phase Measurements

L. Gratton and B. Pervan, *Illinois Institute of Technology*

ABSTRACT

The Federal Aviation Administration is currently developing the Local Area Augmentation System (LAAS) to transition from the current instrument landing system to satellite based navigation. Due to the single frequency nature of the current LAAS architecture for Category I approaches, spatial ionospheric decorrelation contributes significantly to the differential ranging error. During days of normal ionospheric activity, the LAAS Ground Facility (LGF) broadcasts a conservative standard deviation of the spatial ionospheric gradient (σ_{vig}) to LAAS users. Under these normal circumstances, navigation integrity is ensured by incorporating σ_{vig} into the computation of position domain protection levels. However, anomalies exhibiting abrupt changes in the ionospheric gradient have been observed during ionospheric storms in October and November 2003. Therefore, monitoring algorithms are necessary for LAAS to detect these hazardous ionospheric anomalies.

A three parameter (front width, gradient, and front speed) ionospheric threat model has been proposed and significant research has been devoted to the development and analysis of LGF and airborne code-carrier divergence monitors in the past. However, there are limitations on the effectiveness of these monitors, as they depend on the rate of change of the delay with time. The most hazardous threat in this regard is a static ionospheric wave front. In previous work a differential carrier phase Receiver Autonomous Integrity Monitoring (RAIM) monitor to detect this threat was introduced.

This work analyzes detection capabilities of the RAIM monitor for the whole spectrum of fronts within the threat model by showing what combinations of widths and gradients are detectable, and what is the associated availability cost to ensure detectability.

Having the results in terms of combinations of fronts and widths is very advantageous, as it gives insight to the performance of this monitor when combined with a ground baseline monitor. It also provides an idea of how the availability would change with adjustments to the threat model.

A new way of evaluating the availability is presented, using the actual GPS constellation in the sky for the full year 2004.

The availability loss incurred by the implementation of the carrier phase RAIM monitor is presented for different locations in the US. It is shown that this loss is tolerable for most width-gradient combinations. It is also shown it is tolerable for all width-gradients combinations if the monitor only operates during a storm alarm. The availability gain in implementing a baseline ground monitor in conjunction with the RAIM monitor is also provided.

INTRODUCTION

The Federal Aviation Administration is currently developing its Differential GPS (DGPS) type implementation, the Local Area Augmentation System (LAAS) to transition from the current instrument landing system to satellite based navigation. Due to the single frequency nature of the current LAAS architecture, spatial ionospheric decorrelation between the LAAS Ground Facilities (LGF) antenna and the user contributes significantly to differential ranging errors. During days of normal ionospheric activity, the LGF broadcasts a conservative standard deviation of the spatial ionospheric gradient (σ_{vig}) to LAAS users. Under these normal circumstances, navigation integrity is ensured by incorporating σ_{vig} into the computation of position domain protection levels. However, anomalies exhibiting

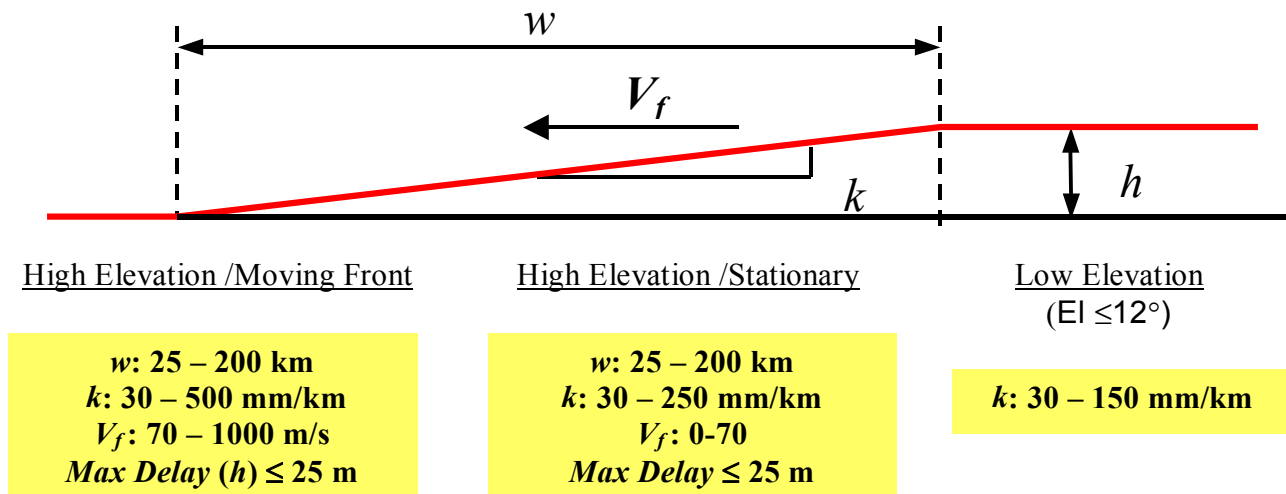


Figure 1: Ionospheric front model and threat space

abrupt changes in the ionospheric gradient have been observed during ionospheric storms in October and November 2003. During these occurrences, the ionospheric effect not eliminated by the broadcast range correction can potentially have a magnitude of tens of meters instead of the nominal centimeter level differences. Therefore, effective monitoring algorithms are necessary for LAAS to detect these hazardous ionospheric anomalies without affecting the system's availability and continuity significantly.

Ionospheric fronts are very difficult to model, as the dynamics of their formation and change with time are not fully understood, and the quantity of data affected by ionospheric fronts to analyze is limited. Stanford University developed a model that describes the front by its effect (delay) on the signal, and thus allows the front to be defined with only a few parameters, simplifying the analysis [1]. These parameters are the front width (w), the front vertical gradient (k), the front height (h , derived from w and k), and the front's velocity. By considering the available data from various ionospheric storms, reasonable boundaries were defined for these parameters, obtaining a threat space. A sketch of the model and the parameter values for the threat space are shown in figure 1.

Detection of these types of threats has been studied using ground and airborne variations of carrier-code divergence monitors. These monitors can mitigate the integrity risk for certain parts of the threat space, but as they depend on the rate of change of the delays, they do not work for slow varying fronts, or stationary fronts.

Two monitors are discussed in this paper. The first one is airborne, and is described in detail. It is a particular implementation of the Residual Autonomous Integrity

Monitor (RAIM) using the very precise carrier phase measurements. The second one is a ground monitor, using baselines between the existing antennas at the LGF to detect the ionospheric front gradient. This monitor is not analyzed in the paper; instead, the consequences on the availability (assuming such monitor is implemented) are described. This work intends to complete the results presented in [2], providing a detailed description of what combinations of widths and gradients for a static ionospheric front are detectable, and what is the associated availability cost to ensure detectability.

Having the results in terms of combinations of gradients and widths is very advantageous, as it gives insight to the performance of this monitor when combined with a ground baseline monitor. It also gives an idea of how the availability would change with adjustments to the threat model. This detailed approach gives a deeper understanding of how well the proposed monitors are providing risk mitigation for stationary ionospheric fronts threats.

The purpose of the monitors is not to detect an ionospheric storm, but to detect if the storm is affecting a particular runway of an LGF site. This means that the availability losses from the monitors presented in this paper might apply only during a storm if there is a reliable ionospheric storm alarm system implemented. It is also worth noting that the hazardous situation for LAAS is not for the LGF and the user being in a high signal delay zone of a front, but when the delay at the LGF and the user's position is significantly different. This is why a failure on only one satellite at a time is considered, as the likelihood of two satellites simultaneously being on the edge of the front (as seen from the LGF) is considered negligible. This assumption is supported by the observed data [3].

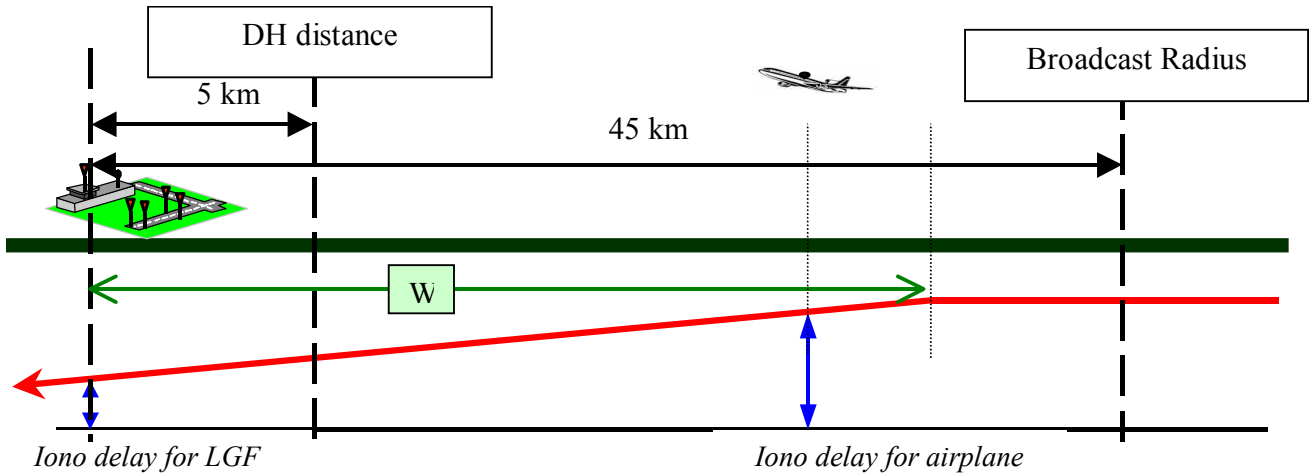


Figure 2: Approach with ionospheric front present

The variable w considered in this analysis is not the physical width of the front, but the width of the front that lies between the LGF antenna and the aircraft. That is why, even though a physical front smaller than 25 km is not in the threat space, the lower limit for w is set to 0. This can be observed in figure 2, where the width is represented by the green line starting at the LGF antenna, even though a part of the front not affecting the approach continues beyond the LGF to the left.

DIFFERENTIAL CARRIER PHASE RAIM MONITOR

The monitor works in two phases. Before initiating the approach, the user performs a geometry screening based on the probability of missed detection given a storm (P_{MD}). If the geometry passes this test, at the LGF Broadcast Radius distance (x_{BR}) the user will compute a single difference user (A) - LGF (G) carrier phase measurement for each satellite i :

$$\phi_i^{SD0} = \phi_i^{A0} - \phi_i^{G0} \quad (1)$$

as it moves closer to the LGF, the user generates a double difference measurement

$$\phi_i = \phi_i^{SD} - \phi_i^{SD0} \quad (2)$$

using a second differential carrier phase measurement; being the Decision Height distance (x_{DH}) the last point to detect a failure. This implementation uses the precise carrier phase to take differential measurements, taking advantage of the baseline formed by the airplane as it executes its approach. The values used in this analysis for x_{BR} and x_{DH} are 45 km and 5 km respectively. It must be stated that for the user to be able to compute these measurements, the LGF would need to broadcast carrier phase corrections (LAAS message Type 6).

Using the computed Line Of Sight unit vectors (LOS), the user will obtain a residual vector as:

$$\begin{bmatrix} r_1 \\ r_2 \\ \vdots \\ r_n \end{bmatrix} = \begin{bmatrix} \phi_1 \\ \phi_2 \\ \vdots \\ \phi_n \end{bmatrix} - \begin{bmatrix} -LOS_1 & 1 \\ -LOS_2 & 1 \\ \vdots & \vdots \\ -LOS_n & 1 \end{bmatrix} \begin{bmatrix} \Delta\hat{x} \\ v \end{bmatrix} = \phi - H\hat{u} \quad (3)$$

where the differential position vector $\Delta\hat{x}$ (in this case the vector with origin in the airplane's position at x_{BR} and ending in the x_{DH} position), and the clock bias v are obtained from:

$$\hat{u} = (H^T V^{-1} H)^{-1} H^T V^{-1} \phi \quad (4)$$

with V being a time (t) changing diagonal weighting matrix whose elements are computed as:

$$(\sigma_i^t)^2 = 2\sigma_{SD}^2 + (\sigma_{vig} \times \Delta z_i^t \times Ob_i^t)^2 \quad (5)$$

σ_{SD} , is the single difference carrier phase measurement standard deviation (a nominal value of 1 cm is used in this work);

σ_{vig} , is the fault free vertical ionospheric gradient.

Δz , is the distance between the pierce-points of the two airplane-SV measurement rays (one at BR and one at DH distance), and

Ob , is the obliquity factor.

The time superscript is dropped from now on.

The test statistic for this monitor will be similar to the one in a Residual Autonomous Integrity Monitor (RAIM) implementation: the norm of the residual vector, now weighted using (5):

$$r = \left\| \begin{bmatrix} \frac{r_1}{\sigma_1} & \frac{r_2}{\sigma_2} & \dots & \frac{r_n}{\sigma_n} \end{bmatrix} \right\| \quad (6)$$

A nominal value of 2 mm/km was used for σ_{vig} . Note that if the value selected was not conservative enough, the availability loss and continuity risks would be higher than the ones from the simulation, but not the integrity risk, as the result of this error will only affect the predicted number of false alarms.

RAIM AND THE SLOPE MODIFIER α

In case of a failure caused by an ionospheric storm, its impact on the test statistic r will be [4]:

$$r^I = (I_d - HH^*)_{:,i} (d_{i(DH)} - d_{i(BR)}) \quad (7)$$

where:

- I_d , is the identity matrix
- H^* , is the pseudoinverse of H , weighted with matrix V (4) and;
- d_i , is the bias introduced in the carrier phase single difference measurement for satellite i by the ionospheric front.

The vertical position error caused by the failure will be:

$$\delta x_v^I = H_{3,i}^+ f_{i(DH)}^I \quad (8)$$

where:

- H^+ , is the pseudoinverse of H weighted according to the differential carrier smoothed code specifications for LAAS Cat I [5], and
- f_i^I , is the error accumulated in the differential Hatch filter measurement to satellite i .

Both effects (on the vertical position error and on the residual) have been considered at decision height distance, as it has the most stringent VAL .

The probability of a Missed-Detection (MD) given a failure F^I , (which will be a function of w , k , and the obliquity factor Ob) is:

$$P_{MD} = P(\delta x_v > VAL) \times P(r < T) | F(w, k, Ob) \quad (9)$$

where T is a threshold derived from the tolerable probability of a false alarm applied to the corresponding Chi Square distribution.

In a traditional RAIM approach, (for a generic failure F) the Failure Mode Slope is defined as:

$$FMS \equiv \frac{|\delta x_v^F|}{\|r^F\|} = \frac{|H_{3,i}^+|}{\|(I - HH^+)_{:,i}\|} \frac{F}{F} \quad (10)$$

It is used to determine availability. For each geometry, a plot of vertical error δx_v with respect to the norm of the residual can be generated (figure 3), where the slope of a line is defined by the FMS , and the nominal distribution or fault free “noise” is schematically represented by the ellipses. The location along this line where the P_{MD} is the biggest (darker ellipse in the figure) can be obtained. If that P_{MD} is bigger than the integrity threshold that geometry is discarded.

When Carrier phase RAIM is use to detect ionospheric fronts additional complications need to be considered. A closer look at the vertical position error and the residual r (7) and (8) when there is an ionospheric storm shows that the magnitude from F^I affecting r :

$$\Delta d_i^I = d_{i(DH)} - d_{i(BR)} = (w - x_{DH}) \times k \times Ob \quad (11)$$

and the magnitude affecting δx_v :

$$f_{i(DH)}^I = k \times Ob \times \left[x_{DH} + 2v\tau \left(1 - e^{-\frac{w-x_{DH}}{v\tau}} \right) \right] \quad (12)$$

are no longer equal (see [2] for details). Now the failure magnitudes to consider are represented in figure 3 by the whole plane instead of a line. Once the limits in k , w and maximum delay of the threat space are applied, the points to evaluate for a given satellite and geometry become an area in the plane (figure 4). It is obvious that finding the point with the worst P_{MD} is now more difficult. Moreover, it is not the maximum that needs to be found anymore, but the limits of the colored area in figure 4 for which the P_{MD} exceeds the integrity constraint. This approach will give more value to the results, as it will evaluate specifically what type of static fronts can be detected and the availability loss caused by geometry screening for the rest. This provides knowledge of the impact on availability of changes in the threat model, or in the detection capabilities of other monitors that would operate jointly with the RAIM monitor. This will become more evident later in the paper.

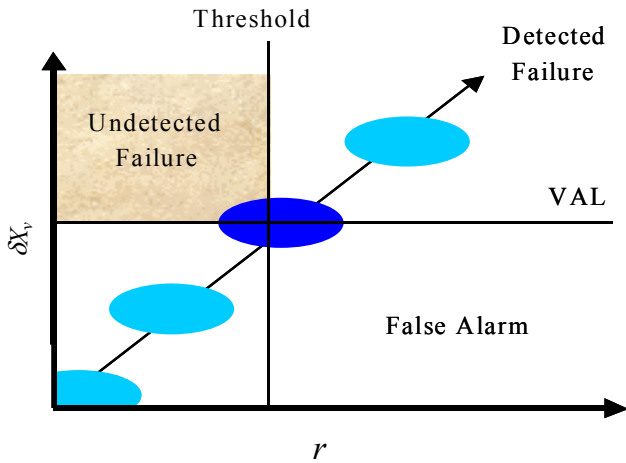


Figure 3: FMS and P_{MD}

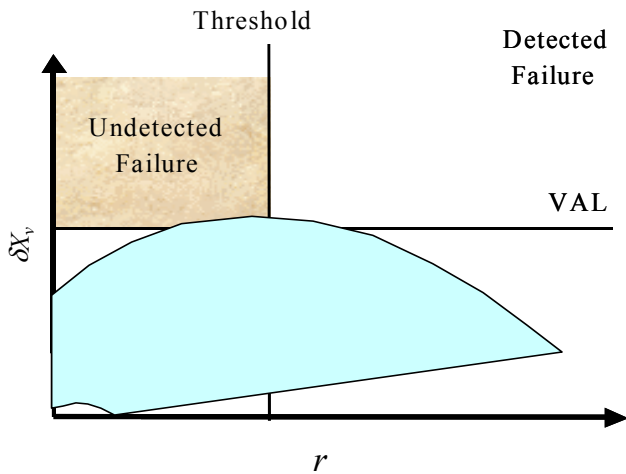


Figure 4: Carrier phase RAIM failure space

w	k	30 mm/km	40 mm/km	50 mm/km	...	250 mm/km
0 km		A	A	A	...	A
10 km		A	A	U	...	U
...	
200 km		A	U	U	...	A

Table 1: Availability matrix for each geometry (example)

w	k	30 mm/km	40 mm/km	50 mm/km	...	200 mm/km
0km		99.99%	99.97%	99.7%	...	99.99%
10km		99.98%	99.97%	82%	...	99.98%
...	
250km		99.80%	99.75%	99.74%	...	99.99%

Table 2: Availability matrix for all geometries (example)

The aim is then to fill a matrix for each geometry (table 1) in which each element (corresponding to a different w, k combination) will be filled with an unavailable result (U) if for any satellite in that geometry the $P_{MD} > 10^{-4}$, and the geometry will be available (A) for that particular threat if for all SV's $P_{MD} < 10^{-4}$. Following this process for each time of interest, adding all matrices (with U's=0 and A's=1), and dividing by the number of geometries, the final availability result is obtained in the form of table 2. The amount of computation needed for this task is enormous, demanding several weeks of code running for each site. This computation burden requires some way of reducing the number of points to evaluate. In order to do this, the advantageous representation of a line from the traditional RAIM has to be recovered. This can be achieved by fixing w . By first defining a slope modifier α_w as:

$$\alpha_w \equiv \left| \frac{f_{i(DH)}^I}{\Delta d_i^I} \right| = \frac{x_{DH} + 2v\tau \left(1 - e^{-\frac{w-x_{DH}}{v\tau}} \right)}{w - x_{DH}} \quad (13)$$

(where the Ob and k are cancelled); the FMS for each w can be redefined as:

$$FMS_w \equiv \frac{|\delta x_v^I|}{\|r^I\|} = \frac{|H_{3,i}^+|}{\|(I - HH^*)_{:,i}\|} \frac{f_i^I}{\Delta d_i^I} \quad (14)$$

$$= \alpha_w \frac{|H_{3,i}^+|}{\|(I - HH^*)_{:,i}\|} \frac{\Delta d_i^I}{\Delta d_i^I}$$

As the failure in the numerator and the denominator are equal again, changing its magnitude will slide the point up and down a line with slope FMS_w for each particular width. The line visualization is recovered and the next section will show how this is used to reduce the computation time from weeks to less than 2 days.

Note that the worst slope SV cannot be selected as in traditional RAIM. This is due to the fact that the threat space changes with a satellite's elevation; so if only the SV with the worst elevation is selected, maybe some (or all) $w-k$ combinations would seem available, but there is another satellite with a better slope, (but a different range of slant delays) that could run into the missed detection zone (figure 5). All satellites should pass the P_{MD} test to make that $w-k$ combination available for that geometry.

The following section provides details on the algorithms implemented to compute the availability. Its reading is not essential for understanding the results.

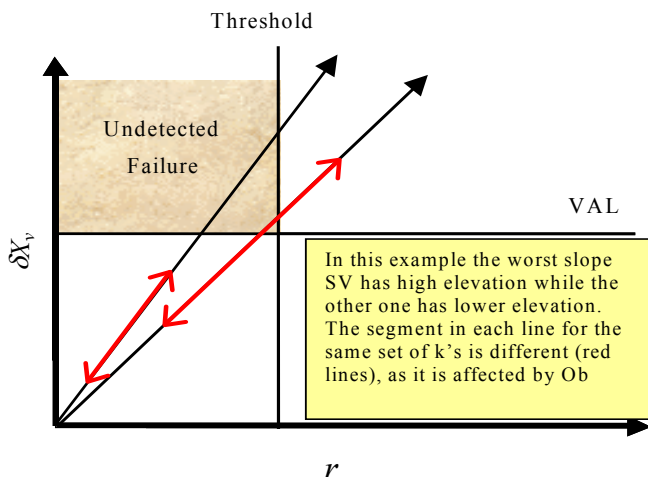


Figure 5: Worst satellite selection

THREAT SPACE COMPUTATION REDUCTION

The basic idea of this section is to reduce to the minimum the number of points in table 1 to be computed, either because the result is obvious without need of computing the P_{MD} , or because it can be deduced from a previously computed result.

The limits of the w to be computed are derived first. On the lower end, for any width thinner than 5 km, there will be no detection (the front will be entirely located after x_{DH}). So, as the position error will only be smaller as w decreases, it is conservative to say:

$$P(MD|f(w < 5km, k)) = P(MD|f(w = 5km, k)) \quad (15)$$

To save computation time on the higher end, let's look at how α_w changes with w (figure 6 shows the values for $43km < w < 60$ km). After $w = 5$ km (from 0 to 5 km $\alpha_w = \infty$) the value decreases rapidly, until $w = 45$ km, then increasing again, until at $w = 200$ km it takes the same value than for $w = 44.9$ km. Since a lower slope reduces the P_{MD} , it is conservative to assume that

$$\alpha_{44.9 < w < 200} = \alpha_{200} \quad (16)$$

It can be seen from (9) and (14) that if α_w is fixed (like it was done above for $44.9 < w < 200$), equal values of Δd_i^I will produce equal values for P_{MD} . So once the availability has been computed for all k 's with $w = 200$ km,

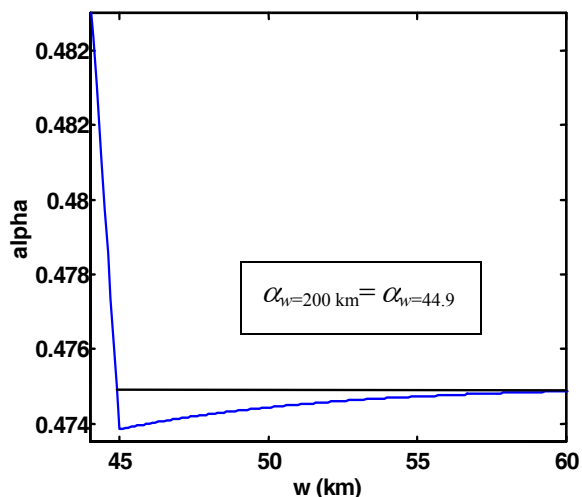


Figure 6: Values of α_w

the availability for $44.9 < w < 200$ can be obtained without any computation by looking at the already known values on the right hand side of:

$$P(MD|f(w, k)) = P(MD|f(200km, k_{equiv})) \quad (17)$$

where:

$$k_{equiv} = \frac{k(w - x_{DH})}{200km - x_{DH}} \quad (18)$$

is the gradient that will produce the same Δd_i^I when combined with $w = 200$ km than the Δd_i^I corresponding to the evaluated w, k pair. So for each geometry, and each satellite, only $5km < w < 44.9$ km, and $w = 200$ km need to be computed.

Reducing the k space to be evaluated is more complex, as it will change with each geometry and satellite. The P_{MD} is the product of two numbers (9), but if it is assumed that all failures will cause a $\delta x_v^I > VAL$, the Non Central Chi² *cdf* of the residual alone will determine the P_{MD} . The limit formula

$$P_{MDallowed} = 10^{-4} = P(D_{dof} < T | DELTA_{high}^{dof}) \quad (19)$$

can be used to find the non-centrality parameter $DELTA_{high}^{dof}$ that causes a *cdf* = 10-4 for a Non Central

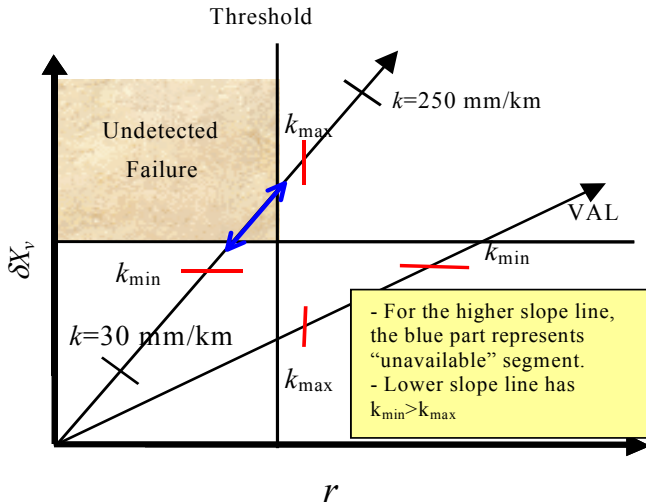


Figure 7: Search Limits

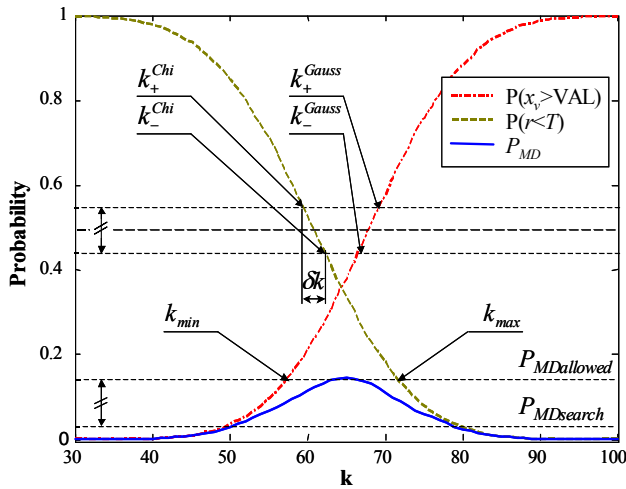


Figure 8: Search interval δk

Chi Square distributed D_{dof} with dof degrees of freedom. The $P_{MDallowed}$ is set from the allocated integrity risk for the monitor (10^{-4} in this case). The Non-centrality parameter affecting the RAIM residual distribution is given by the denominator squared in (14), so using the value obtained in (19) the maximum value of k to be evaluated is given by (figures 7 and 8):

$$k_{max}(H, w) = \frac{1}{Ob} \sqrt{\frac{DELTA_{high}^{dof}}{(I - HH^*)_{i,i} (w - X_{DH})^2}} \quad (20)$$

[Notice that that only the $(I - HH^*)_{i,i}$ element is needed, as it is the term multiplying the failure, all the other elements of that vector are multiplied by 0's, since F^l affects only one satellite at a time].

Similar reasoning can be used to obtain the minimum k to be evaluated. By assuming there is no detection, the bias μ_{low} that gives a $cdf=10^{-4}$ for a gaussian distributed $D_{gaussian}$ can be computed:

$$P_{MD} = 10^{-4} = P(D_{gaussian} > VAL | (\mu_{low}, \sigma)) \quad (21)$$

with

$$\sigma = \sqrt{(H^T R^{-1} H)_{3,3}} \quad (22)$$

R being the weighting matrix mentioned in (8). [Note: The Gaussian distribution has 2 tails corresponding to $P(\delta x_v > VAL)$ and $P(\delta x_v < -VAL)$, but by looking at several million cases, it was found that, even with no failure present, the maximum value for the second tail is smaller than 1.5×10^{-8} so it can be safely ignored]. Now, as the bias in the P_{MD} evaluation comes from the numerator in (14), the minimum k to be evaluated is obtained as:

$$k_{min}(H, w) = \frac{\mu_{low}}{H_{3,i}^+ \alpha_{(w)} (w - X_{DH}) \times Ob} \quad (23)$$

The main advantage of finding these limits relies in finding satellites for which no computation needs to be done at all. As all satellites must be evaluated, many will have a very low slope, in that case, $k_{min} > k_{max}$. (figure 7). So without any further work, it is obvious that that satellite will not cause any availability loss for that w

For those satellites with $k_{min} < k_{max}$ the search for the unavailable segment in each line is done in two steps (figure 7). First it must be determined if there is a segment for which $P_{MD} > 10^{-4}$, if that is the case, the limits of that segment must be found. This second step does not demand much time, but what generally consumes most of the search time is being able to discard the possibility that such segment exists. The key is to find the biggest interval δk that will guarantee a segment of unavailability is not being overlooked. The worst case from the search point of view is when the P_{MD} curve barely touches the $P_{MDallowed}$ value (figure 8), as for that case an infinitely small δk would need to be adopted not to miss it. To avoid that problem, the search will look for a $P_{MDsearch} < P_{MDallowed}$, (in this case $P_{MDsearch}=10^{-5}$ was used). So now the challenge is finding a minimum δk that will guarantee that if a case with $P_{MD} > P_{MDsearch}$ has not been found, it is certain that there will not be a $P_{MD} > P_{MDallowed}$. To be conservative, the value δk is obtained at the steepest segment for each curve independently (in the vicinity of $P_{MD}=0.5$), assuming the other curve has a value of 1 in

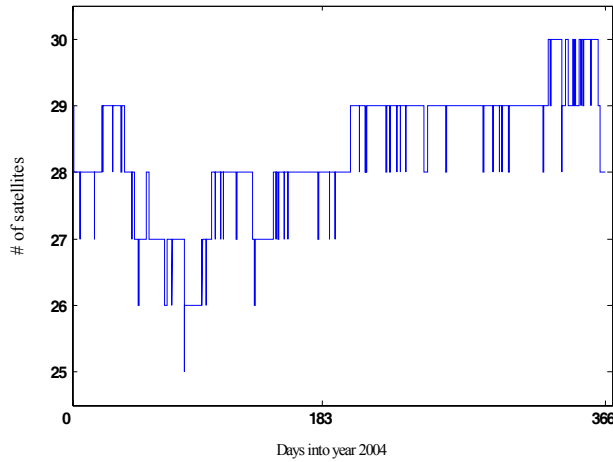


Figure 9: Healthy GPS SV's year 2004

that region (any other value would make the change smoother, allowing a larger δk). The values of k limiting the desired P_{MD} segment [from $0.5 - (P_{MDallowed} - P_{MDsearch}) / 2$ to $0.5 + (P_{MDallowed} - P_{MDsearch}) / 2$] can be found by the same procedure used to find k_{min} and k_{max} . For the χ^2 distribution:

$$P_{MD} = 0.5 \pm 0.5 \times 0.9 \times 10^{-5} = P(D_{dof} < T | DELTA_{\pm}^{dof}) \quad (24)$$

and

$$k_{\pm}^{Chi}(H, w) = \frac{1}{Ob} \sqrt{\frac{DELTA_{\pm}^{dof}}{(I - HH^*)_{i,i} (w - X_{DH})^2}} \quad (25)$$

then:

$$\delta k^{Chi} = k_{-}^{Chi} - k_{+}^{Chi} \quad (26)$$

With the same reasoning, and using formulas (21) and (23) for the gaussian curve, with the corresponding values:

$$\delta k^{Gauss} = k_{+}^{Gauss} - k_{-}^{Gauss} \quad (27)$$

finally:

$$\delta k = \min(\delta k^{Gauss}, k^{Chi}) \quad (28)$$

Figure 8 will help the reader visualize this procedure [$P_{MDallowed}$ and $P_{MDsearch}$ are out of scale to make the plot readable]. In summary, as the search for an unavailable segment progresses, the interval between the points where the P_{MD} is computed is made smaller and smaller. If by the time it reaches a value of δk there is no $P_{MD} > 10^{-5}$, it is certain there will be no $P_{MD} > 10^{-4}$ anywhere in the line. This means no point in the row in table 1 corresponding

to the particular w being computed needs to be changed to "unavailable" and the search for the next w can start without further computation.

CONSTELLATION

Before showing the results, it is appropriate to explain the constellation used. It introduces a new way of evaluating the availability by looking at the effect of the monitor using the real GPS constellation, with the actual outages.

The period considered was the whole year 2004. For that period, the NANUs were consulted, establishing all cases in which a satellite was added or taken out of the GPS constellation (figure 9). For each lapse of time without changes in the number of SV's, a set of broadcast ephemerides close to the middle point of that period was used to generate the satellite positions for that lapse of time. This has the advantage of giving a real sense of the impact of the monitor implementation with the actual satellites in space and their outages. It also has the added value, that for segments of time bigger than a sidereal day, only the availability matrices (table 1) for the first 24 hours need to be computed as the results will be repeated in a daily basis

RESULTS

The unavailability in percentage for 3 of the sites evaluated is shown in figure 10. On the right, is a detail of the w - k combinations that cause bigger unavailability. There is a cutoff at 150 mm/km for some sites, due to the threat model for low elevation satellites (figure 1).

It can be seen that for smaller values of k and bigger values of w , the availability loss is small. For values of $k < 100$ mm/km, and $w > 42$ km, the unavailability ranges from 0 to 0.01 %. The first column in table 3 shows the maximum unavailability caused by a given combination of w and k (the most intense red spot for each site in figure 10). The second column shows the total availability loss if all geometries for which any w - k combination gives a $P_{MD} > 10^{-4}$ are discarded. These numbers are the equivalent of the total availability loss if LAAS relies only on the RAIM monitor to detect all kinds of static ionospheric fronts. It is important to note that this impact on availability would only occur during a storm. The alarm for the storm would come from WAAS. [Another interesting option is using NASA's satellites located between the earth and the sun. ACE, in a halo type orbit around the L1 libration point, can provide accurate information determining if a Coronal Mass Ejection (CME) from the sun will affect the earth's ionosphere with at least an hour warning, while SOHO can provide a less accurate early warning a few days before the CME impacts the atmosphere. Once STEREO is in orbit, the

number of false early warnings will be significantly reduced [6]]. As was stated in the introduction, physical fronts thinner than 25 km do not exist in the threat space. This implies that when a threat with $w < 25$ km is considered, part of that front must necessarily be on top of the LGF (figure 2). It is useful to analyze then how much the availability would improve if the RAIM monitor

operates in conjunction with an LGF monitor. As the carrier RAIM monitor detects the front by observing the gradient in the baseline formed by its own movement (figure 2), the LGF can detect it by using the baselines formed with its different redundant antennas [2]. If it is assumed that an LGF monitor can detect any front that is at least 500 m into the LGF ($x_{top} > 500m$) (the equivalent

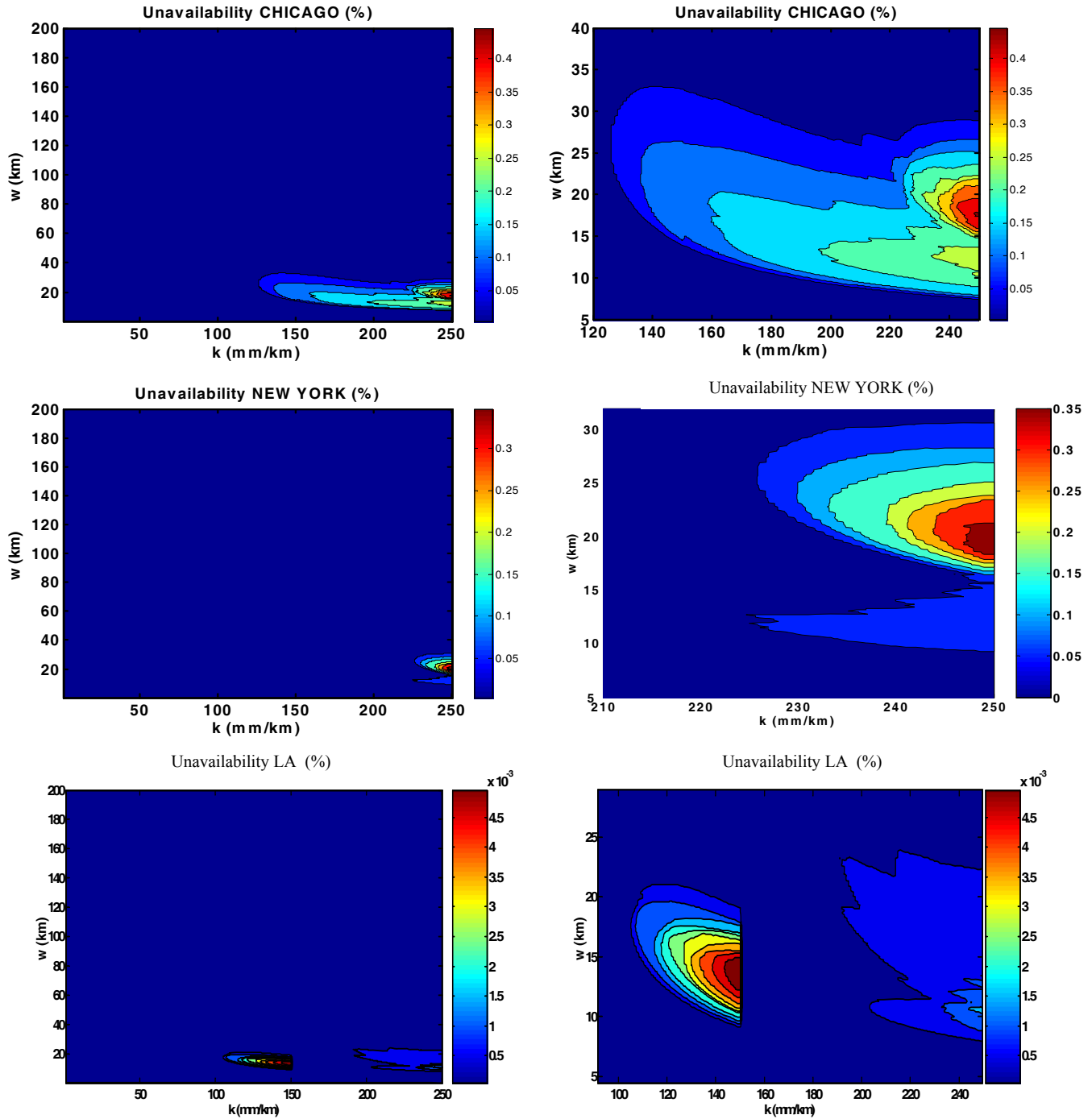


Figure 10 Unavailability results

	Max	Total	$x_{top} < 500$ or $k < 150$
Chicago	0.456	0.654	0.307
Dallas	0.227	0.455	0.179
New York	0.383	0.486	0.202
L.A.	0.541	0.799	0.595
Miami	0.183	0.276	0.093
Seattle	0.132	0.192	0.07

Table 3: Final results

of $w < 24.5$ km for the threats being considered), with a gradient $k > 150$ mm/km, all w - k combinations that meet these two conditions are considered "available". The resulting reduced unavailability with the two monitors operating simultaneously is shown in the 3rd column of table 3. It can be seen that the improvement ranges from 30% to 50% with respect to the RAIM monitor operating alone. Reducing the needed x_{top} to 100 m instead of 500 m did not improve results significantly, nor did the assumption of a better LGF monitor that could detect fronts with $k > 100$ mm/km (with the exception of LA, for which the improvement was more than 90 %, the reason becomes obvious by looking at the corresponding plot in figure 10).

CONCLUSIONS

The static front is the most hazardous type of ionospheric anomaly, as existing monitors cannot detect it. A RAIM type monitor algorithm was described. It takes advantage of the baseline formed by the aircraft's movement during the final approach, and the precision of the carrier phase measurements utilized in its implementation. As a tradeoff, it requires the broadcast of message type 6 (carrier phase corrections), and the evaluation of the P_{MD} for geometry screening is more sophisticated. The computational burden to estimate the availability loss was reduced significantly by using the properties of the distributions for the RAIM residual and the aircraft's position error, making it a realizable task time-wise. A new way of computing the availability loss was

introduced using the actual GPS constellation in the sky during a whole year. Results show that for fronts wider than 42 km or with $k < 100$ mm/km, the availability loss varies from 0 to 0.01 %. Total availability loss during a storm varies from 0.2 to 0.8 % depending on the site. If the RAIM monitor operates in conjunction with an LGF baseline monitor, the unavailability is reduced by 1/3 to 1/2 depending on the site.

ACKNOWLEDGMENTS

The authors wish to acknowledge Sam Pullen and Ming Luo for their useful comments on the threat model and the specifications to be used, Mathieu Joerger for his comments and help with the plots, and the Federal Aviation Administration for sponsoring this research.

REFERENCES

- [1] Luo, Ming, L., Pullen, S., Walter, T., and Enge, P., "Ionosphere Spatial Gradient Threat for LAAS: Mitigation and Tolerable Threat Space", Institute of Navigation's National Technical Meeting, San Diego CA 2004
- [2] Gratton, L., Chan, F., Pervan, B., "Algorithms for Airborne Ionospheric Front Detection in LAAS Using Carrier Phase and INS Measurements", Institute of Navigation's National Technical Meeting, San Diego CA 2005
- [3] Private conversation with Dr. Sam Pullen, October 2004
- [4] Pervan, B., "Navigation Integrity for Aircraft Precision Landing using the Global Position Landing" Ph.D. Thesis, Dept. Of Aeronautics and Astronautics, Stanford University, Stanford, March 1996
- [5] "Minimum Aviation System Performance Standards for the Local Area Augmentation System" RTCA Paper No.037-98/SC159-778, February 1998
- [6] "The Sun and The Heliosphere in Three Dimensions", Report of the NASA Science Definition Team for the STEREO Mission, 1997